PHYSICSAccess Research Paper
ISSN Online: 2756-3898, ISSN Print: 2714-500X https://doi.org/10.47514/phyaccess.2023.3.2.005

Exploring the Physical Properties of Tungsten Diselenide (WSe_2): A First Principle Approach

Mohammed Adamu[1], Shuaibu Alhassan[1], Sadiq G Abdu[1] and Muhammed M Aliyu[1]

[1] Department of Physics, Kaduna State University, Kaduna, PMB 2339, Kaduna, Nigeria

Corresponding E-mail: adamu.mohammed@kasu.edu.ng

Received 19-08-2023
Accepted for publication 20-09-2023
Published 20-09-2023

Abstract

The physical properties of crystalline compounds are highly essential for predicting their applications in various nanodevices. Density functional theory is very useful in that regard. Herein, some physical properties such as structural stability, and electronic, optical and mechanical properties of two-phase bulk WSe_2 have been comparatively investigated by first principle calculations. Band structure calculations elucidate that the materials are indirect band gap semiconductors having band gap energy in the range 1-1.5 eV. It was observed that the hexagonal crystal has higher absorption coefficients compared to the trigonal phase. Analysis of elastic constants of the materials carried out using the Born criteria method indicates that all systems are mechanically stable at room temperature. Our findings are in close agreement with the previous experimental and theoretical results, this further suggests that the materials are promising in optoelectronics applications.

Keywords: DFT; Hexagonal phase WSe_2; Trigonal phase WSe_2; Effective mass; Born criteria.

I. INTRODUCTION

Tungsten Diselenide (WSe2) is an inorganic crystalline compound belonging to the family of transition metal dichalcogenide (TMDC)[1] represented with general formula MX2, where M stands for transition metal and X is chalcogenides (S, Se and Te) [2]. WSe_2 is chemically stable [3], p-type in nature and has an indirect band gap [4, 5]. It takes hexagonal and trigonal phases. Recently research on TMDC materials has shown that dimensionality plays a very important role in determining the basic physical properties of these compounds [6]. In this regard, a monolayer or two-dimension, bilayer and a few layers of TMDCs have been successfully synthesized [7]. The bulk and few layers of WSe2 have found applications in many devices and electronic components, such as solar cells, rechargeable lithium batteries, photodetectors, transistors and light emitting diode (LED) [8]. It is also used as a lubricant. Among TMDCs WSe_2 has been a very attractive crystalline compound in recent years due to its precious physical properties such as good electron mobility, structural stability, and band gap in the visible light spectrum (400 to 700 nm) [9]. Reference [10] reported a GW and PBE method to examine the band structure of bulk WSe_2. More recently, [6] investigated the electronic and optical properties of hexagonal bulk WSe_2 ($p6_3/mmc$) using DFT, utilizing PBE-GGA. They confirmed the semiconducting nature of this compound. Though the physical properties of the bulk hexagonal phase of WSe_2 are well studied, the trigonal phase has received far less attention and its properties are not completely explored.

In this paper, we used first-principles density functional theory (DFT) to comparatively investigate the structural, electronic, elastic and optical properties of the hexagonal with space group ($p6_3/mmc$), group number 164 and trigonal-phase having space group ($p\bar{3}m1$) and group number 187 bulk WSe_2.

II. COMPUTATIONAL DETAILS

In this study, we used the projector augmented plane wave (PAW) numerical method to solve the Kohn-Sham equation within the framework of density functional theory (DFT) implemented in Quantum ESPRESSO code [11] to investigate the hexagonal and trigonal phases of bulk tungsten Diselenide (WSe_2) with 6 and 3 atoms respectively. First principle functional theory non-spin polarized calculations [12] were carried out in the generalized gradient approximation for crystals as given by Pardew, Burke and Ernzerhof (GGA-PBE) [13]. For integrals smearing has been employed and precisely the Maxfesse-Paxton smearing method [14], for both the two crystalline compounds. Monkhost-Pack Scheme has been adopted for the Brillouin zone integration [15] with 12x12x3 k-points grids for WSe_2, in the electronic properties calculation. The WSe_2 structures were optimized using Broyden-Fletcher-Goldfarb-Shannon (BFGS) algorithms[16]. The atomic positions were fully relaxed until the forces acting on the atoms were below 0.001 eV/Å.

III. RESULTS AND DISCUSSION

A. Structural properties

The equilibrium structural ground state parameters of the two-phase bulk WSe_2 compounds, such as the lattice constants, the structural optimization in the quantum espresso code has been carried out using Perdew Burke Ernzerhof generalized gradient approximation (PBE-GGA) by minimizing the total energy with respect to the volume of the unit cell. The geometric structures of the compounds are hexagonal and trigonal as shown in Fig. 1a and b, Fig. 1c shows the Brillouin zone used for k-path in band structure calculations for the considered crystal compounds. Fig. 2 depicts the energy as a function of the volume of the hexagonal and trigonal phases of the considered compounds. The calculated total energies are fitted to Murnaghan's equation of state to obtain the ground state equilibrium lattice constant. The total ground state energies for the hexagonal and trigonal structures are -106.207316 and -53.103372Ry per supercell which confirm the structural stability of the considered systems. The calculated and experimental lattice constants, bulk modulus and its pressure derivative are listed in Table I. It is seen that the lattice constants obtained with PBE-GGA agree with other similar calculations. The calculated bulk modulus in Hexagonal WSe_2, 59.7 GPa, is 15% smaller than that of trigonal.

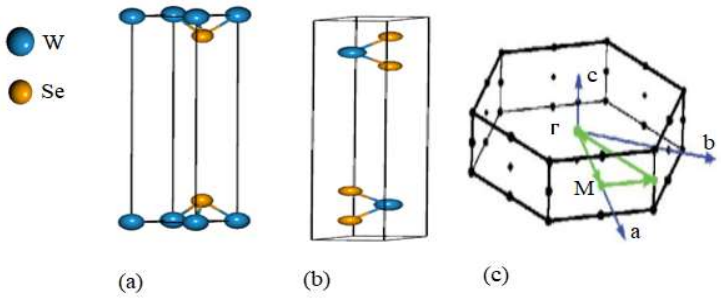

Fig. 1 Primitive cells of Bulk (a) Trigonal, (b) Hexagonal WSe_2 structures and (c) Brillouin zone used for k-path in band structure plots.

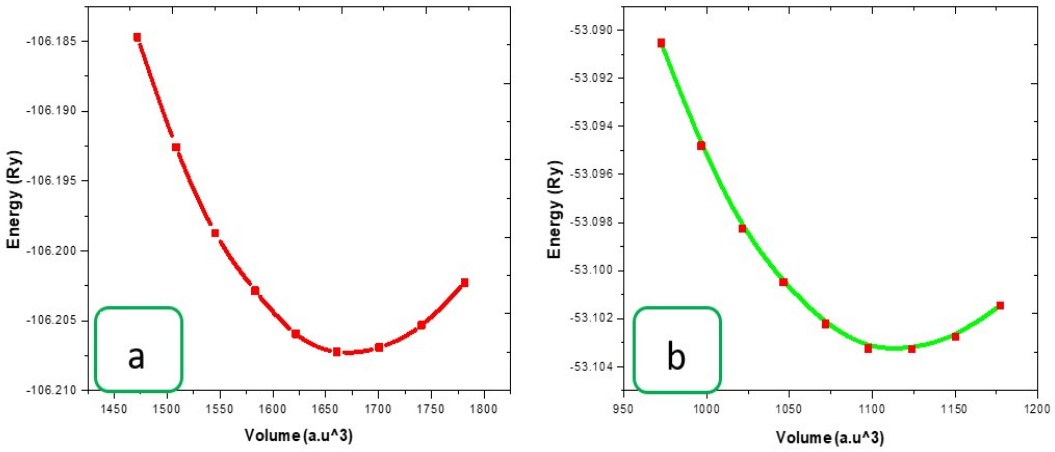

Fig. 2 Energy volume curves of Bulk (a) Hexagonal and (b) Trigonal WSe_2 structures.

Table I. Calculated equilibrium lattice constants for Bulk Hexagonal and Trigonal WSe_2 structures by using PBE-GGA.

Ref.	a (Å)	c (Å)	B(GPa)	B	E_0 (Ry)
Hexagonal WSe_2	3.356	12.743	23.15	2.492	-106.20731
*Hexagonal WSe_2	3.216 [10]	13.170 [10]			
	3.628 [17]	12.980 [17]			
Trigonal WSe_2	3.543	12.876	17.10	2.878	-53.10337
*Trigonal WSe_2	---	---			

*PBE GGA calculations

B. Electronic Properties

We use the optimized structures of the considered materials to carry out the electronic properties' calculations. In electronic band structure calculation, we used PBE-GGA. The band structures of the two compounds were calculated along high-symmetry directions of the Brillouin zone Γ-M-K-Γ and the fermi energy level is set at 0 eV. The calculated band structures for the considered crystals are shown in Fig. 3. Both phases of bulk WSe_2 are indirect band gap semiconductors. The calculated band gap energies are 1.4 and 1.5 eV for hexagonal and trigonal respectively, these values together with experimental values are listed in Table II. These results show that DFT has overestimated the band gaps. This is due to the inherent drawback of GGA/LDA functional courses by self-interaction errors [18, 19]. Fig. 4 illustrated the density of state plots for the considered compounds, they all confirmed the band gap energies of the materials as observed in band structure plots.

Electron acquires masses, different from its rest mass (m_o) when accelerated in a magnetic or electric field. This mass is known as effective mass (m*) and has a negative value in the valence band and a positive value in the conduction band. By using the curve fitting technique, the effective mass of the electron in conduction band minimum (CBM) and hole in valence band maximum (VBM) were obtained from the E-K plot (Band structure) of the compounds by applying (1).

$$m^* = \hbar^2 \left[\frac{dk^2}{d^2E}\right] \quad (1)$$

Where $\hbar = h/2\pi$, h is planks constant, k is wavevector and E is energy.

Table III shows the calculated effective masses of electrons and holes for the two phases in the unit of electron rest mass (m_o). Reference [20] has reported small effective masses of electron holes for perovskite/HfS_2 and attributed it to the efficient separation of photon-generated excitons. This is what makes them attractive for photovoltaic applications.

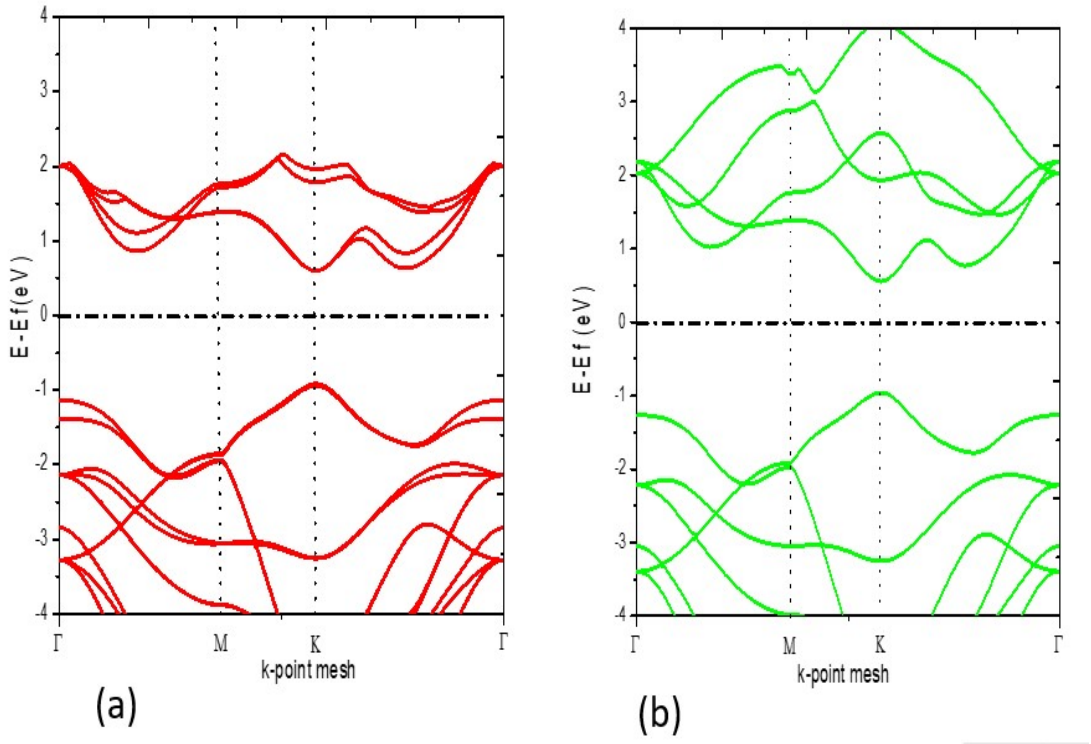

Fig. 3 Band structure of Bulk (a) Hexagonal and (b) Trigonal WSe_2 crystalline compounds.

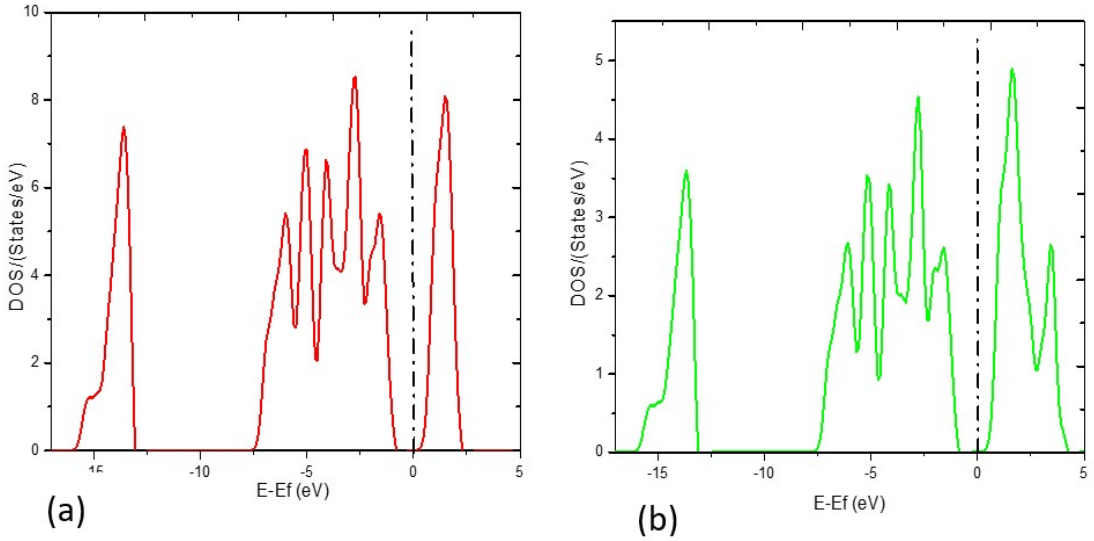

Fig. 4 Density of state of Bulk (a) Hexagonal and (b) Trigonal WSe_2 crystalline compounds.

Table II. Calculate band gap for Hexagonal and Trigonal bulk WSe_2 Structures.

Compound	Band Gap (eV)		
	This work	DFT (PBE-GGA)	Experimental
Hexagonal WSe_2	1.4	1.00 [6], 1.33 [10]	1.75 [10]
Trigonal WSe_2	1.5	1.10 [17]	

Table III. Calculated effective mass of electrons and holes for Hexagonal and Trigonal bulk WSe_2 Structures.

Compound	Effective mass (GGA-PBE)	
	m^*_e(Kg)	m^*_h(Kg)
Hexagonal WSe_2	$0.104m_o$	$0.137m_o$
Trigonal WSe_2	$0.099m_o$	$0.133m_o$

*Experimental

C. *Optical Properties*

The crystal's response to incident radiation determined its application for optoelectronic devices and nanoelectronic components [21]. This prompted the study of the optical properties of crystalline materials, such as absorption coefficient, optical conductivity, refractive index, reflectivity etc. These parameters can be determined from the dielectric tensor ε(ω) given by [22].

$$\varepsilon(\omega) = \varepsilon_1(\omega) + i\varepsilon_2(\omega) \quad (2)$$

The imaginary part $\varepsilon_2(\omega)$) can be calculated from the Kubo-Greenwood equation expressed as (3)[23],

$$\varepsilon_2(\omega) = \frac{2\pi e^2}{\Omega\varepsilon_o}\sum_{k,v,c}|\langle\Psi_k^c|u.r|\Psi_k^v\rangle|^2\,\delta(E_k^c - E_k^v - E) \quad (3)$$

While the real part $\varepsilon_1(\omega)$ of the dielectric tensor can be obtain from the imaginary component using the Kramer-Kronig equation given by,

$$\varepsilon_1(\omega) = 1 + \left(\frac{2}{\pi}\right)\int_0^\infty d\omega\,\frac{\omega'^2\varepsilon_2(\omega')}{\omega'^2-\omega^2} \quad (4)$$

$$\alpha(\omega) = \sqrt{2}\omega\left[\sqrt{\{\varepsilon_1(\omega)\}^2 + \{\varepsilon_2(\omega)\}^2} - \varepsilon_1(\omega)\right]^{\frac{1}{2}} \quad (5)$$

$$\sigma(\omega) = \frac{\omega\varepsilon_2(\omega)}{4\pi} \quad (6)$$

$$n = \sqrt{\left(\frac{\sqrt{\{\varepsilon_1(\omega)\}^2+\{\varepsilon_2(\omega)\}^2}+\varepsilon_1(\omega)}{2}\right)} \quad (7)$$

Where ω is the frequency of phonon, Ω is the unit cell volume, u is the unit vector, e is the electron charge, Ψ_k^c and Ψ_k^v are the wavefunctions for conduction and valence band electrons respectively at k, $\alpha(\omega)$ is the absorption coefficient, $\sigma(\omega)$ optical conductivity and n is the refractive index of the material.

We investigated the optical properties in the incident photon energy range of zero to 20 eV. Fig. 5a and b show the plots of the real part of the dielectric tensor $\varepsilon_1(\omega)$ against energy and imaginary part $\varepsilon_2(\omega)$ against energy for the hexagonal system respectively. The graphs show that there is no significant difference along the x and y-directions for the values of both components. This is also observed with trigonal WSe_2 structure Fig. 5c and d, this could be attributed to their lattice constants, where a is equal to b but not equal to lattice parameter c. The values of the static real part of the tensor $\varepsilon_1(0)$ in the x and y-direction are 5.93 while in the z-direction is 2.40 for the hexagonal compound, as recorded in Table IV. The trigonal phase $\varepsilon_1(0)$ in the x and y-direction has a value of 4.19, and 2.35 in the z-direction. This confirmed that both structures are anisotropic.

Table IV. Calculated static dielectric ε1(0) for Hexagonal and Trigonal WSe_2 bulk structures in three polarization directions.

Compound	$\varepsilon_1(0)$		
	E‖x	E‖y	E‖z
Hexagonal WSe_2	5.92954670	5.92954670	2.40032769
Trigonal WSe_2	4.19333697	4.19333697	2.34844347

As we compared to the hexagonal, the dielectric behaviour for trigonal shown in Fig. 5 is slightly the same. However, the values of the dielectric tensor for hexagonal are much larger than trigonal. The zero-frequency limit $\varepsilon_1(0)$ shown in the Fig. 5a gives the static dielectric tensor. The calculated static dielectric functions of both systems for different polarization directions are given in Table IV, the calculated dielectric tensors of the hexagonal are a little bit higher than trigonal.
Fig. 6a shows the variation of the refractive index and 6b absorption coefficient in the energy range from zero to 20 eV for the hexagonal compound. Whereas Fig. 6c and 6d show the same for the trigonal phase. In the absorption plot in Fig. 6b and 6d the first maxima occur at 1.48 eV and 1.53 eV corresponding with band gap energies of the materials earlier stated in Table II.

Table V. Calculated static refractive index n (0) for Hexagonal and Trigonal WSe_2 bulk structures in three polarization directions.

Compound	n(0)		
	E‖x	E‖y	E‖z
Hexagonal WSe_2	2.43785851	2.43785851	1.55387872
Trigonal WSe_2	2.04971319	2.04971319	1.51912046

Fig. 6c and d depict the plots of refractive index with photon energy. From these graphs, we extract the static refractive indices (n (0)) of the two-phase WSe_2 as seen in Table V.

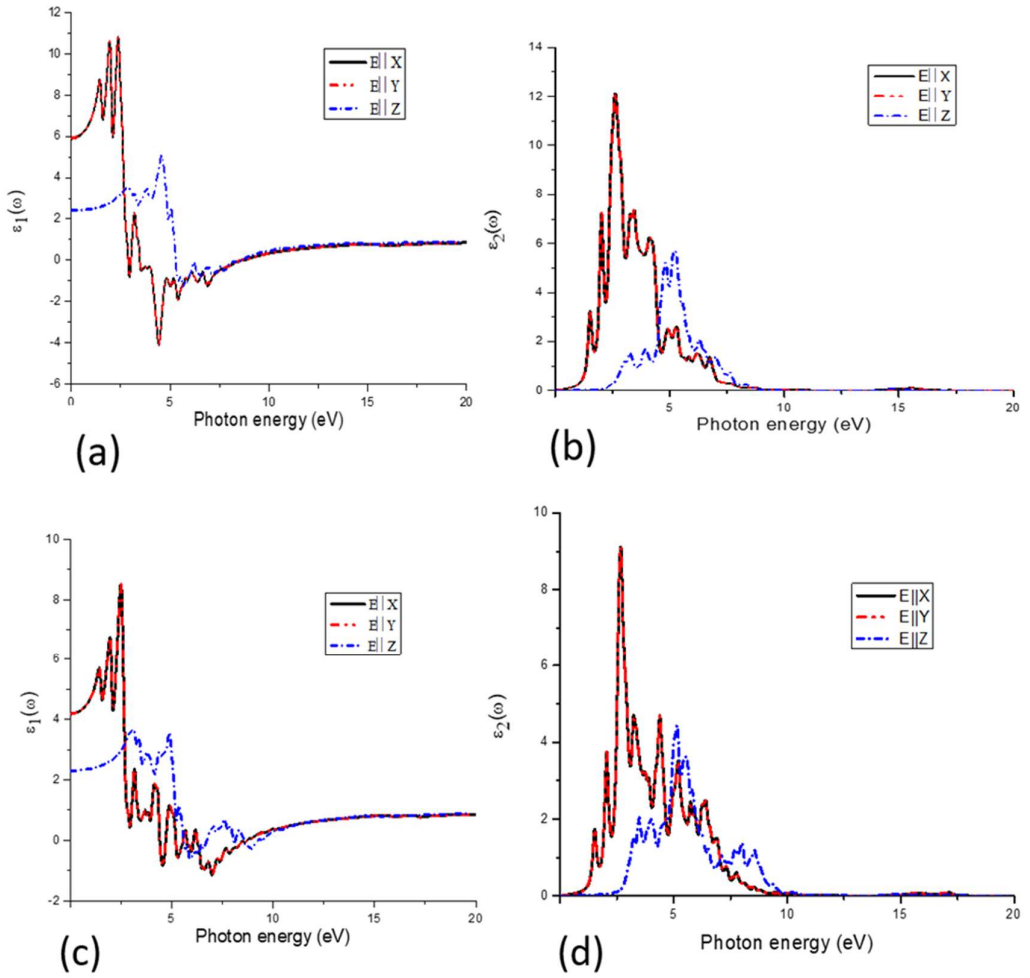

Fig. 5 Dielectric tensors of Bulk (a and b) Hexagonal and (c and d) Trigonal WSe_2 crystalline compounds.

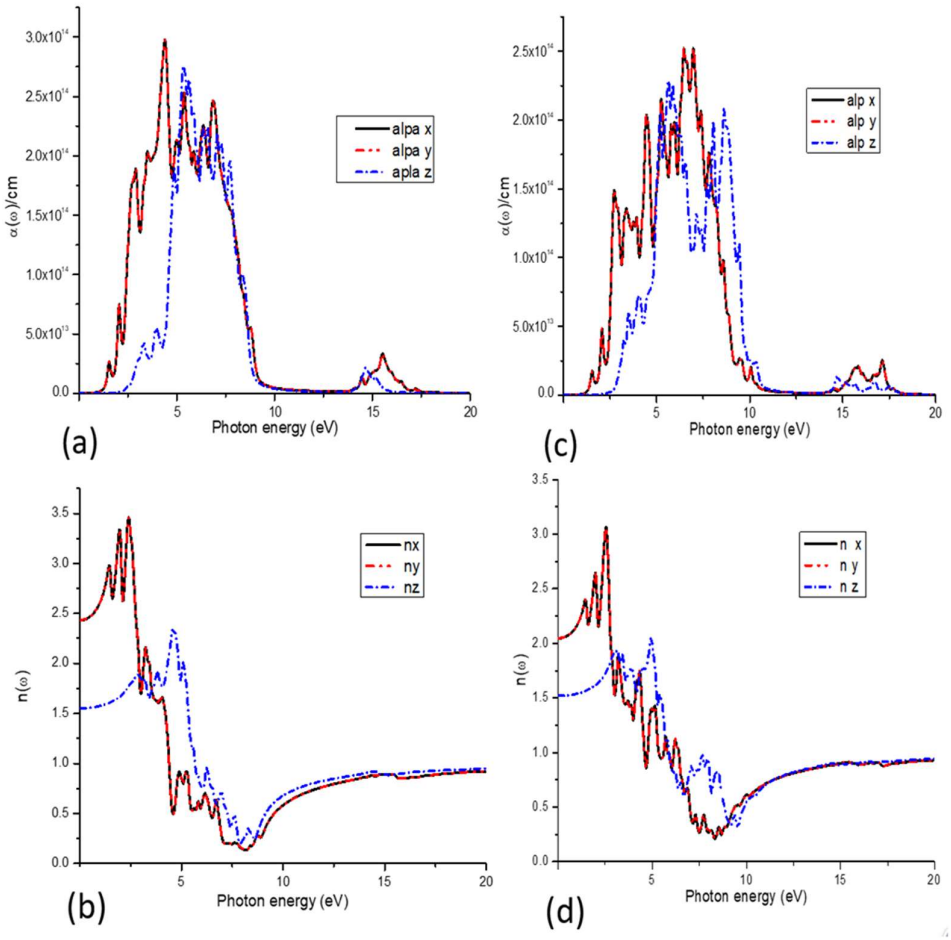

Fig. 6 Absorption (α (ω)) and refractive index (n(ω)) plots of Bulk (a and b) Hexagonal and (c and d) Trigonal WSe_2 crystalline compounds.

D. Mechanical Properties

Elastic constant and elastic moduli provide the ground for understanding the mechanical properties of crystalline solids such as brittleness [12], stability, hardness, ductility, and other mechanical characteristics. The calculated elastic constant for the considered bulk structures within the framework of PBE GGA functional is presented in Table VI. These results are compared with the theoretical and experimental findings. The mechanical stability of bulk materials under isotropic pressure can be analyzed using the popular Born stability criteria [9] given as,

$$C_{11} > 0, C_{33} > 0, C_{44} > 0 \quad (8)$$

$$(C_{11} - C_{12}) > 0 \quad (9)$$

$$(C_{11} + C_{12}) > C_{33} - 2C_{13}^2 \quad (10)$$

The independent elastic constant is given by,

$$C_{66} = (C_{11} - C_{12})^2 \quad (11)$$

All the studied materials satisfy the Born mechanical stability limitations as illustrated by (8)-(11). Furthermore, the table demonstrates that the elastic constants for all the materials are all positive indicating that they are all stable [9] [24].

Table VI. Elastic Constant of Bulk Hexagonal and Trigonal WSe_2 within GGA-PBE Functional.

Elastic constant (Kbar)	GGA-PBE	
	Hexagonal WSe_2	Trigonal WSe_2
C_{11}	801.996	587.88043
C_{12}	172.489	117.82029
C_{13}	13.858	23.48457
C_{33}	13.738	55.07496
C_{44}	21.988	10.92863
C_{66}	396,279	220,956

1) Hardness and Elastic moduli

The mechanical properties of a material can be determined from its calculated elastic constants. The machinability of a material can be calculated by dividing its bulk modulus by its elastic constant C_{44}. It was established that the higher the value of the ratio $\left(\frac{B}{C_{44}}\right)$ the better the machinability [9]. Herein, we have calculated the bulk modulus (B), the shear modulus (G) and the Young's modulus (Y) for the individual C_{ij} for all the considered materials. According to Pugh's rule, the ratio (G/B) can be used to determine the brittleness or ductility of the material compound. This rule states that if $\frac{G}{B} > 0.57$ then the material is ductile else it behaves as brittle. In this work, the calculated values of $\frac{G}{B}$ indicate that all the materials have shown a ductile nature. Reference [25] reported that material ductility can be determined using Poisson's ratio. They elucidated that Poisson's ratio greater than 0.25 means the material is ductile, and anything less than 0.25 indicates a brittle material.

For hexagonal structures, the bulk (B_v) and shear (G_v) moduli can be obtained from (12) and (13) using the elastic constant,

$$B_v = \frac{1}{9}[(2C_{11} + C_{12}) + C_{33} + C_{13}] \quad (12)$$

$$G_v = \frac{1}{30}[C_{11} + C_{12} - 2C_{33} + 4C_{13} + 12C_{44} + C_{66}] \quad (13)$$

Synthesized systems are more often studied in the form of ceramic polycrystalline, hence, it is important to calculate the elastic parameters of the investigated materials systems in their polycrystalline state. To that effect, we use the Vogt-Reuss-Hill approximation, according to which two other essential approximations are utilized, i.e., the Voigt and Reuss approximations. The expressions for the shear and bulk moduli are given by the Reuss model as

$$B_R = \frac{(C_{11}+C_{13})C_{33}-2(C_{13})^2}{C_{11}+C_{12}+2C_{33}-4C_{13}} \quad (14)$$

$$G_R = \frac{5}{2}\frac{\left((C_{11}+C_{12})C_{33}-2(C_{13})^2\right)C_{44}C_{66}}{[3B_vC_{44}C_{66}+\{(C_{11}+C_{12})C_{33}-2(C_{13})^2\}(C_{44}+C_{66})]} \quad (15)$$

The effective modulus of anisotropic polycrystalline crystals is calculated using bulk modulus and the shear modulus, as approximated by Hill [26] is given by,

$$G = \frac{1}{2}(G_v + G_v) \quad (16)$$

$$B = \frac{1}{2}(B_v + B_v) \quad (17)$$

The average and the actual effective moduli above can be used to obtain bulk and shear moduli as approximated by Voigt-Reuss-Hill given by

$$E = \frac{9BG}{3B+G} \quad (18)$$

Now, the Poisson's ratio(v) for polycrystalline material can be given by the expression,

$$v = \frac{3B-2G}{2(3B+G)} \quad (19)$$

2) Crystal Anisotropic Index

The orientation dependency of the elastic moduli is called crystal elastic anisotropy [27, 28]. Anisotropy of a material can be calculated using elastic constant C_{44} as shown in (20) [9]. The anisotropy index has been assigned to crystals for its importance in the design of crystals in science and engineering. Reference [9] reported that $A_{an} = 1.0$ shows an isotropic crystal, while $A_{an} > 1.0$ *or* $A_{an} < 1.0$ indicates anisotropy. In this work, the results presented in Table III suggest that all our crystals are anisotropic by nature.

$$A_{an} = \frac{4C_{44}}{C_{44}+C_{44}+C_{44}} \quad (20)$$

IV. Conclusion

This paper reports a computational description and comparison of structural, electronic, optical and mechanical characteristics of hexagonal and trigonal phase WSe_2 bulk systems using DFT calculations. Our results elucidate shows that the two Polymorphs of the crystal WSe_2 are stable, they are both semiconductors with an indirect band gap between 1-1.5 eV, which agrees well with previous theoretical and experimental findings. The results show that the bandgap of the trigonal is larger than hexagonal. The complex dielectric tensor, absorption spectrum and refractive index were calculated and discussed. Our findings further reveal that the hexagonal's real and imaginary parts are larger than the real and the imaginary parts of the dielectric function of trigonal. The hexagonal has a higher absorption coefficient and refractive index in all three polarization directions. The results further suggested that the two materials are anisotropic and brittle.

Conflict of Interest

The authors declare that they have no known competing financial interests or personal relationships that could have appeared to influence the work reported in this paper.

Acknowledgement

The authors acknowledge the use of the facilities at the Department of Physics, Kaduna State University, Nigeria and the assistance of Dr. Abdullahi Lawal Kubau of the Department of Physics, Federal College of Education Zaria.

Reference

[1] S. Roy and P. Bermel, "Electronic and optical properties of ultra-thin 2D tungsten disulfide for photovoltaic applications". *Solar Energy Materials and Solar Cells,* vol. 174, pp. 370-379, 2018.

[2] L. Loh, Z. Zhang, M. Bosman, and G. Eda, "Substitutional doping in 2D transition metal dichalcogenides". *Nano Research,* vol. 14, pp. 1668-1681, 2021.

[3] S. O. A. Ahmad *et al.*, "Application of two-dimensional materials in perovskite solar cells:

recent progress, challenges, and prospective solutions". *Journal of Materials Chemistry C,* vol. 9, no. 40, pp. 14065-14092, 2021.

[4] J. Li, L. Jia, X. Zheng, C. Peng, and X. Fu, "Structural and elastic properties of WSe2: first-principles calculations". Journal of Physics: Conference Series, 2020, vol. 1634, no. 1, pp. 012145: IOP Publishing.

[5] Y. Tian, G. Jia, and P. Wu, "First-Principles Study of in Doped in WSe_2," *Available at SSRN 4120244*.

[6] H. Abbadi, S. Malki, and L. El Farh, "Ab initio calculations of structural and electronic properties of WSe2 compound". Materials Today: Proceedings, vol. 31, pp. S130-S133, 2020.

[7] D. H. Jung, Y. J. Oh, Y. S. Nam, and H. Lee, "Effect of layer number on the properties of stable and flexible perovskite solar cells using two-dimensional material". *Journal of Alloys and Compounds,* vol. 850, pp. 156752, 2021.

[8] A. Ali Umar, N. Ain Abd Malek, N. Alias, and A. Anuar Ehsan, 'Two-Dimensional Transition Metal Dichalcogenide as Electron Transport Layer of Perovskite Solar Cells', Chalcogenides - Preparation and Applications. IntechOpen, Jul. 20, 2022. doi: 10.5772/intechopen.103854.

[9] S. A. Yamusa, A. Shaari, and I. Isah, "Structural stability, Electronic and Optical Properties of Bulk MoS_2 Transition Metal Dichalcogenides: A DFT Approach," *J. Appl. Phys,* vol. 14, pp. 40, 2022.

[10] H. Jiang, "Electronic band structures of molybdenum and tungsten dichalcogenides by the GW approach". The Journal of Physical Chemistry C, vol. 116, no. 14, pp. 7664-7671, 2012.

[11] P. Giannozzi *et al.*, "QUANTUM ESPRESSO: a modular and open-source software project for quantum simulations of materials". *Journal of Physics: Condensed matter,* vol. 21, no. 39, p. 395502, 2009.

[12] M. Khanzadeh and G. Alahyarizadeh, "A DFT study on pressure dependency of TiC and ZrC properties: Interconnecting elastic constants, thermodynamic, and mechanical properties". *Ceramics International,* vol. 47, no. 7, pp. 9990-10005, 2021.

[13] J. P. Perdew, K. Burke, and M. Ernzerhof, "Generalized gradient approximation made simple". Physical review letters, vol. 77, no. 18, pp. 3865, 1996.

[14] A. A. Masanawa, A. Shuaibu, M. M. Aliyu, and I. Magaji, "First Principle Investigation on Electronic Properties of Cationic and Anionic CO-Alloyed Cu2ZnSnS4 Kesterite Material". Physics access, sp.iss.2022.1, pp. 13-16, 2022.

[15] H. J. Monkhorst and J. D. Pack, "Special points for Brillouin-zone integrations". *Physical Review B,* vol. 13, no. 12, pp. 5188, 1976.

[16] W. Zhao, "A Broyden–Fletcher–Goldfarb–Shanno algorithm for reliability-based design optimization". *Applied Mathematical Modelling,* vol. 92, pp. 447-465, 2021.

[17] W. Dawson and D. Bullett, "Electronic structure and crystallography of MoTe2 and WTe2". Journal of Physics C: Solid State Physics, vol. 20, no. 36, pp. 6159, 1987.

[18] W. Wu, X. Wang, and Z. Zeng, "The magnetic properties of pressurized CsV 3 Sb 5 calculated by using a hybrid functional". Physical Chemistry Chemical Physics, vol. 24, no. 30, pp. 18179-18184, 2022.

[19] K. S. Shirali, "Tuning Properties of Topological Insulators: An Ab-initio Approach". Ph.D. dissertation, Dept. of Phy. and Astro., Louisiana St. Univ., Baton Rouge, Louisiana St, USA, 2022.

[20] D. Singh and R. Ahuja, "Two-dimensional perovskite/HfS2 van der Waals heterostructure as an absorber material for photovoltaic applications". ACS Applied Energy Materials, vol. 5, no. 2, pp. 2300-2307, 2022.

[21] M. Roknuzzaman, J. A. Alarco, H. Wang, and K. K. Ostrikov, "Structural, electronic and optical properties of lead-free antimony-copper based hybrid double perovskites for photovoltaics and optoelectronics by first-principles calculations". *Computational Materials Science,* vol. 186, pp. 110009, 2021

[22] F. Ghasemi, R. Taghavimendi, and A. Bakhshayeshi, "Electronic and optical properties of monolayer and the bulk of PtSe 2". *Optical and Quantum Electronics,* vol. 52, pp. 1-14, 2020.

[23] A. Radzwan, A. Lawal, A. Shaari, I. M. Chiromawa, S. T. Ahams, and R. Ahmed, "First-principles calculations of structural, electronic, and optical properties for Ni-doped Sb2S3". Computational Condensed Matter, vol. 24, pp. e00477, 2020.

[24] C. F. Cline, H. L. Dunegan, and G. W. Henderson, "Elastic constants of hexagonal BeO, ZnS, and CdSe". Journal of Applied

Physics, vol. 38, no. 4, pp. 1944-1948, 1967.
[25] J. Du *et al.*, "Strain engineering in 2D material-based flexible optoelectronics". *Small Methods,* vol. 5, no. 1, pp. 2000919, 2021.
[26] Y. Pan and D. Pu, "Hydrogen embrittlement of C40 transition-metal disilicides". Journal of Materials Research, vol. 34, no. 18, pp. 3163-3172, 2019.
[27] L. W. Finger, "Physical properties of crystals, their representation by tensors and matrices," ed: Wiley Online Library, 1983.
[28] R. Hill, "The elastic behaviour of a crystalline aggregate". *Proceedings of the Physical Society. Section A,* vol. 65, no. 5, pp. 349, 1952.